JOURNAL of the MEXICAN CHEMICAL SOCIETY

https://www.jmcs.org.mx/

Article

Open Access

J. Mex. Chem. Soc. **2026**, *70(1):e2378*

Received October 14th, 2024
Accepted March 19th, 2025

http://dx.doi.org/10.29356/jmcs.v70i1.2378
e-location ID: 2378

Keywords:
Thiazole, density functional theory, molecular docking, anticancer, anticholinesterase reactivity

Palabras clave:
Tiazol, teoría del funcional de la densidad, acoplamiento molecular, anticancerígeno, reactividad anticolinesterásica

***Corresponding author:**
Selvarengan Paranthaman
email: psrengan@hotmail.com

ISSN-e 2594-0317

Investigation of Structure, Reactivity, and Biological Activity of Thiazole-Containing Compounds: A Computational Study

Selvarengan Paranthaman[1]*, Saranya Gurumoorthy[1], Karthikeyan Asokan[1,3], Abiram Angamuthu[2,4]

[1]Department of Physics and International Research Centre, Kalasalingam Academy of Research and Education (Deemed to be University), Krishnankoil 626 126, India.
[2]Department of Physics, PSG College of Arts and Science, Coimbatore 641 014, India.
[3]Department of Physics, M. Kumarasamy College of Engineering, Karur - 639 113, India.
[4]Department of Physics, Rathinam Technical Campus, Coimbatore - 641 021, India.

Abstract. Herein, the structure, stability, reactivity, and biological activity of recently synthesized thiazole-containing compounds are evaluated using density functional theory (DFT), molecular docking, and molecular dynamics (MD) techniques. All the selected thiazole-containing compounds are optimized using DFT (B3LYP/def2-TZVPP) method. The DFT reactivity parameters such as energy gap, chemical hardness, chemical potential, ionization potential, electron affinity, electronegativity, softness, and electrophilicity index are calculated. Our calculations indicate that the thiazole-containing compound M1 shows significant structural stability and reactivity. Our physicochemical and pharmacokinetic studies suggest that the selected thiazole-containing compounds possess a drug-like nature. The antibacterial, anticancer, anticholinergic, and antifungal activity of the selected thiazole-containing compounds are investigated using molecular docking and dynamics methods. Our docking studies revealed that M1 shows higher binding affinity with the selected protein targets, which confirms their biological activity. Similarly, M6, M9, and M10 possess lesser binding energy among the selected thiazole-containing compounds. Our MD simulations

J. Mex. Chem. Soc. **2026**, *70(1):e2378*
Regular Issue

ISSN-e 2594-0317

show that the ligand M1 strongly interacts with the 1M17 protein. shows higher binding affinity with the selected protein targets, which confirms their biological activity. Similarly, M6, M9, and M10 possess lesser binding energy among the selected thiazole-containing compounds. Our MD simulations show that the ligand M1 strongly interacts with the 1M17 protein. This is further evidence that the ligand M1 is a promising candidate for the development of new drugs against deadly pathogens.

Resumen. En este trabajo, se evalúan la estructura, estabilidad, reactividad y actividad biológica de compuestos que contienen tiazol recientemente sintetizados mediante la teoría del funcional de la densidad (DFT), acoplamiento molecular y técnicas de dinámica molecular (MD). Todos los compuestos seleccionados que contienen tiazol se optimizan mediante el método DFT B3LYP/def2-TZVPP. Se calculan los parámetros de reactividad de la DFT, como la brecha de energía, la dureza química, el potencial químico, el potencial de ionización, la afinidad electrónica, la electronegatividad, la suavidad y el índice de electrofilicidad. Nuestros cálculos indican que el compuesto M1, que contiene tiazol, muestra una estabilidad estructural y una reactividad significativas. Nuestros estudios fisicoquímicos y farmacocinéticos sugieren que los compuestos que contienen tiazol seleccionados poseen una naturaleza similar a la de un fármaco. Se investiga la actividad antibacteriana, anticancerígena, anticolinérgica y antifúngica de los compuestos que contienen tiazol seleccionados mediante métodos de acoplamiento molecular y de dinámica. Nuestros estudios de acoplamiento revelaron que M1 presenta una mayor afinidad de unión con las proteínas diana seleccionadas, lo que confirma su actividad biológica. De igual manera, M6, M9 y M10 poseen una menor energía de unión entre los compuestos que contienen los tiazoles seleccionados. Nuestras simulaciones muestran que el ligando M1 interactúa de forma fuerte con la proteína 1M17. Esto constituye una prueba más de que el ligando M1 es un candidato prometedor para el desarrollo de nuevos fármacos contra patógenos mortales.

Introduction

Thiazole is a class of heterocyclic organic compounds that have garnered significant attention in the scientific community due to its wide range of applications. This can be attributed to the presence of sulfur with its chemical structure (Fig. 1). It must be noted that the first antibiotics used to treat microbial infection contain thiazole i.e. penicillin. Further, the biological significance of thiazole is due to the structural similarity of thiazole with the protein imidazole group. Many researchers have utilized thiazole-containing compounds to develop novel drugs. Over the past few decades, numerous thiazole-based derivatives have been investigated to evaluate their biological and pharmacological potential [1,2]. To be precise, the synthesis of thiazole derivatives got attention due to their diverse biological activities, including anti-inflammatory [3–5], antimicrobial [6–11], antitumor [12–14], analgesic, [15,16], anti-HIV [17], antidiabetic [18], antioxidant [19,20], COX/LOX inhibitory [21,22], and antileishmanial [23,24]. There are many drugs with thiazole, such as antiviral (brecanavir, and ritonavir); antitumor (dasatinib, and tiazofurin); antibacterial agents, including sulfathiazole [25], anti-infectious (nitazoxanide) [26]; antifungal agents, such as ravuconazole [27], and penicillin [28]; and abafungin [29], myxothiazol [30], and ethaboxam [31] are available for the treatment. Even though an enormous number of studies were found in the literature on thiazole derivatives, still a rigorous search is going on to identify the biologically active thiazole derivatives. This is because of less effectiveness of common antibiotics against deadly diseases.

Drug resistance is becoming a big global concern these days. For example, Staphylococcus aureus and Neisseria gonorrhoeae (the cause of gonorrhea) are now almost always resistant to benzylpenicillin [32,33]. Previously, these infections were usually controlled by penicillin, a thiazole derivative. Due to fatal infections' resistance to certain well-known medications, pharmaceutical and medicinal chemists are constantly in search of new potential drugs that could be an alternative to known drugs. However, experimental challenges such as crystallization, purification, and limitations in synthesis methods hinder the search for new drugs and the study of their applicability. Hence, in the present investigation computational techniques such as density functional theory (DFT), molecular docking, and molecular dynamics to explore the potential biological applications of the recently synthesized thiazole derivatives. In the last few decades, density functional theory (DFT) methods have been

J. Mex. Chem. Soc. **2026**, *70(1):e2378*
Regular Issue

ISSN-e 2594-0317

widely used to study the atomic and molecular properties of various molecular systems. It could be used as an alternative to high-cost experimental techniques.

To understand the biological activity of the selected thiazole-containing compounds, the antimicrobial (antibacterial, antifungal, and antiviral), anticancer, and anticholinergic activities of the recently synthesized thiazole-containing compounds are evaluated. The present study is threefold. First, recently synthesized thiazole-containing compounds are obtained from the popular chemical database PubChem. Second, the geometrical parameters of the selected thiazole-containing compounds are optimized using density functional theory (DFT). In particular, reactivity parameters of the selected thiazole-containing compounds are obtained using DFT calculations. Third, biological activities such as anticancer, antimicrobial (antibacterial, antifungal), and anticholinesterase of the selected thiazole-containing compounds are investigated using molecular docking technique. That is, by blocking the active sites of the protein targets by using the selected thiazole-containing compounds. Understandably, the selected thiazole-containing compounds were well-reported in the literature. The earlier researchers have studied those selected thiazole-containing compounds. However, the objective of their study was limited to one or two biological activities, for ex. antimicrobial activity, antifungal, or anticancer etc. This could be due to the high cost of experimental techniques. Earlier researchers have investigated the biological activity of imidazole–thiazole hybrids using experimental techniques (34, 35). To the best of our knowledge, our study is a systematic cost-effective computational study at the molecular level to evaluate the potential biological applications of thiazole-containing compounds. Our study will be helpful to the experimentalists and theoreticians in designing and developing new drugs for the treatment of persistent deadly pathogens.

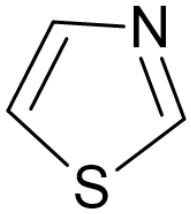

Fig. 1. Molecular structure of Thiazole.

Computational details

In the present investigation, 52 thiazole-containing compounds are obtained from PubChem to study their biological significance (Table S1). Those thiazole-containing compounds were recently reported in PubChem. Among them, 12 thiazole-containing compounds are identified as bioactive compounds. Molinspiration web tool is used to calculate their bioactivity score [36]. The results are shown in Table S2. The selected thiazole-containing compounds are named M1, M2, etc., along with their PubChem IDs for convenience. Further, density functional theory calculations are performed on the selected thiazole-containing compounds. That is, the molecular structure of the selected thiazole-containing compounds is optimized using the B3LYP/def2-TZVPP basis set. The initial geometries of the selected thiazole-containing compounds are taken from PubChem [37]. Earlier studies have mentioned that combining B3LYP with def2-TZVPP yields better results for bio-organic systems [38]. The vibrational frequencies of the selected thiazole-containing compounds are calculated using the above method to understand the stability of the selected compounds. The scaling factor of 0.963 is used to obtain scaled vibrational frequencies [39]. Previous studies have demonstrated that this factor effectively accounts for the systematic overestimation of vibrational frequencies by density functional theory calculations, ensuring better agreement with experimental data. Using this factor improves the reliability of the computed vibrational frequencies for bioorganic molecules, such as the thiazole derivatives analyzed in this study. The DFT reactivity parameters such as highest occupied molecular orbital (E_{HOMO}) and the lowest unoccupied molecular orbital (E_{LUMO}) energies, energy gap (E_g), chemical hardness (η), chemical potential (μ), and electrophilicity index (ω) are calculated for all the selected systems by using,

http://dx.doi.org/10.29356/jmcs.v70i1.2378

J. Mex. Chem. Soc. **2026**, *70(1):e2378*
Regular Issue

ISSN-e 2594-0317

$$E_g = E_{LUMO} - E_{HOMO} \quad (1)$$

$$\eta = \frac{I - A}{2} \quad (2)$$

$$\mu = -\frac{I + A}{2} \quad (3)$$

$$\omega = \frac{\mu^2}{2\eta} \quad (4)$$

Where E_{LUMO} and E_{HOMO} are the lowest unoccupied molecular orbital and highest occupied molecular orbital energies, respectively, $I = -E_{HOMO}$ and $A = -E_{LUMO}$, where I and A represent the ionization potential and electron affinity of the molecule, respectively. All the DFT calculations are performed using the ORCA 5.0 program [40].

The molecular docking study is performed for all the selected thiazole-containing compounds against various protein targets for antibacterial, anticancer, anticholinergic, and antifungal activity. The selected protein targets are given in Table 1. Standard cleaning procedures have been completed before docking. The proteins are prepared using Biovia Discovery Studio [41] by subtracting cofactors, water molecules, and metal ions and adding charges and polar hydrogen atoms. The prepared proteins are loaded into PyRx and converted into macromolecules. Twelve thiazole-containing compounds were converted into PDB format for input to AutoDock Vina in PyRx. Finally, the proteins and thiazole-containing compounds were converted into PDBQT and ready for docking. All of the screened compounds were then further docked with protein targets using the PyRx program [42].

Molecular dynamics (MD) simulations were carried out with the GROMACS 2022.5 package [43] using the CHARMM36 force field [44], which gives complete information on the interactions between atoms. MD is a highly efficient, cost-effective, and more powerful classical approach compared to less intensive statistical approaches like the molecular docking method. It gives valuable insights into the behavior of complex biological macromolecular systems. This cannot be obtainable from high-cost experimental techniques. In the present study, MD simulations are performed to investigate the 1M17 protein and its docked complexes of 1M17-M1. TIP3P water molecules are used to solvate the system in a triclinic box. To achieve stand salt concentrations i.e. to neutralize the system, Na and Cl ions are added. To ensure system stability, an equilibration process is conducted to employ a position-restrained dynamics simulation (NVT) at 300 K, lasting for 1000 ps with a leapfrog algorithm [45,46]. After this step, a production run was performed on the entire system for 20 ns, with constant temperature and pressure conditions. These MD simulations allowed us to understand the behavior of the protein and docked protein-ligand complexes. All the standard statistical analyses such as Root-Mean-Square-Deviation (RMSD), Radius-of-Gyration (Rg), and Root-Mean-Square-Fluctuation (RMSF), and calculation of hydrogen bonds are performed using GROMACS utility programs.

Table 1. Selected protein targets and their PDB IDs.

Biological Activity	**Protein name**	**PDB IDs**
Antibacterial activity[a]	*E. Coli* gyrase	1KZN
	Thymidylate Kinase	4QGG
	E. coli Primase	1DDE
	E. coli MurA	3KR6
	E. coli MurB	2Q85

J. Mex. Chem. Soc. **2026**, *70(1):e2378*
Regular Issue

ISSN-e 2594-0317

Biological Activity	Protein name	PDB IDs
Anticancer activity[b]	EGFR Kinase	1M17
	Tyrosine Kinase	1T46
Anticholinergic activity[c]	Human Acetylcholinesterase	4EY7
	Human butyrylcholinesterase	4BDS
Antifungal activity[a]	DNA TopoIV	1S16
	CYP51 of *C. albicans*	5V5Z

[a][54], [b][58]. [c][62,63]

Results and discussion

Structure of thiazole-containing compounds

The selected thiazole-containing compounds are optimized using density functional theory. In particular, all the selected thiazole-containing compounds are optimized using B3LYP functional with a def2-TZVPP basis set. The optimized 3d structure of the selected thiazole-containing compounds is shown in Fig. 2. From Fig. 2, it can be seen that the thiazole group present in all the selected compounds, which are favorable for the formation of non-covalent interactions such as cation-π, anion-π, alkyl-π interactions. These interactions play a vital role in various biological processes like drug-receptor interactions, enzyme-substrate interactions, protein-protein interactions, etc., [47]. Further, the presence of amino group (-NH) in the thiazole moiety forms hydrogen bond interaction with amino acid residues in bacterial protein targets. Earlier studies have mentioned that the amino groups enhance the bioactivity of thiazole-containing compounds [48]. Apart from the thiazole group, this amino group is present in M3, M5, M6, M7, M8, M11, M12 compounds. Most of the thiazole-containing compounds consist of benzene rings (M1, M2, M3, M7, M8, M11). This functional group is favorable for the formation of π-π, and π-σ interactions with the amino acid residues in the protein targets considered in this study. Similarly, Imidazole, and -NO_2 group are present in M1. These groups are favorable for the formation of hydrogen bond interaction. M2 and M12 consist of the naphthalene group. Peptide bond and halogen (Br) are present in M2. The phosphate group is present in M10. Similarly, M7 and M11 consist of bipyridine groups. These functional groups are favorable for the formation of non-covalent interactions such as cation-π, anion-π, and alkyl-π interactions, as well as hydrogen-bonded interactions. Most of the thiazole-containing compounds consist of amino and carboxylic groups, which are favorable for the formation of hydrogen bond interaction. Similarly, the indanone group is present in M2, which is favorable for the formation of cation-π, anion-π, and alkyl-π as well as hydrogen bond formation. The M4 derivative consists of a polymeric chain, which is not favorable for non-covalent interactions because of its hydrophobic nature. Overall, the functional groups such as thiazole, benzyl, indanone, bipyridine, imidazole, amino and carboxylic groups along with halogens present in the selected thiazole-containing compounds. This indicates that these functional groups could form non-covalent interactions such as cation-π, anion-π, alkyl-π, π-σ, hydrogen bonds, and halogen bonds between the selected residues and amino acid residues in the protein targets. Further, it must be noted that the presence of these functional groups enhances the bioactivity of the selected compounds. For ex. The indanone group plays an important role in donepezil, a standard drug that is used for cholinergic inhibition. The presence of electronegative elements in the hybrids will increase the lipophilicity, which increases the metabolic activity and membrane permeation of the hybrids [49].

http://dx.doi.org/10.29356/jmcs.v70i1.2378

J. Mex. Chem. Soc. **2026**, *70(1):e2378*
Regular Issue

ISSN-e 2594-0317

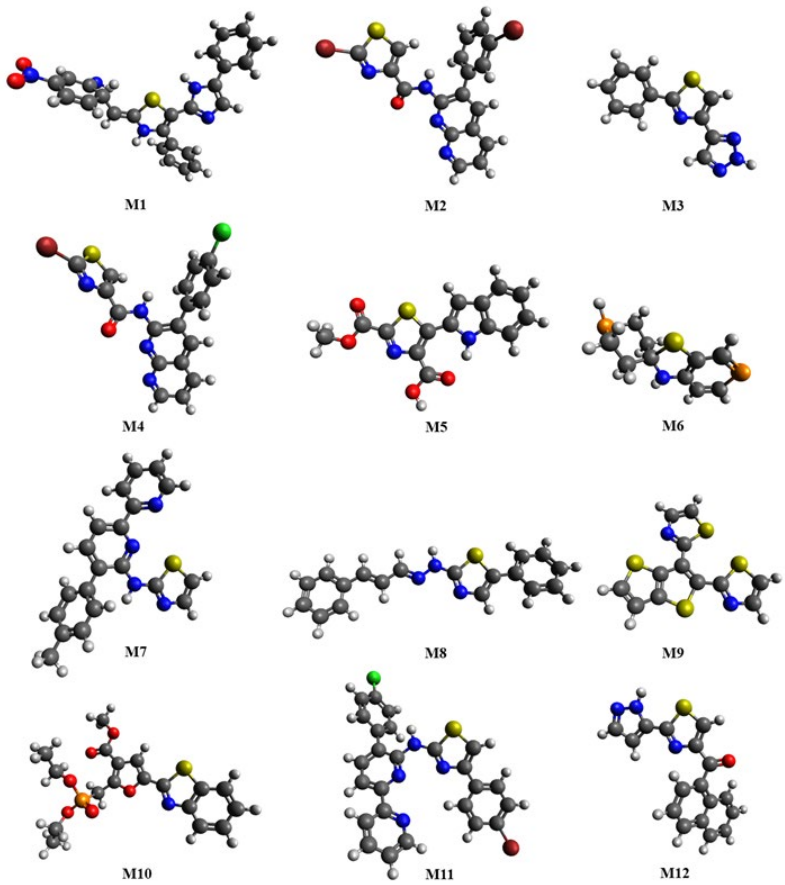

Fig. 2. Optimized (2d) structures of the selected thiazole derivatives.

To validate the selected DFT functional and basis set for our study, the calculated results are compared with the available experimental results. The experimental vibrational frequency and ^{13}C NMR chemical shift are available for a few of the selected ligands. The experimental IR vibrational frequency data is available for ligands M1, M2, M4, M8, and M12. The experimental ^{13}C NMR chemical shift is available for M1, M2, M4, M7, M10, M11 and M12. Among them, experimental ^{13}C NMR chemical shifts with assignments are available for M1 and M10 only. The calculated vibrational frequency, and ^{13}C NMR chemical shifts along with their experimental values are given as the supporting information file (Table S2, Table S3, Table S4). Our calculated vibrational frequency and ^{13}C NMR chemical shifts are comparable with the experimental results. This is evidenced by our correlation studies, which are shown in Fig. 3 for vibrational frequency and Fig. 4 for ^{13}C NMR chemical shift. The R^2 value for all cases is 0.99. This indicates that the calculated values coincide well with the experimental values for vibrational and ^{13}C NMR chemical shifts (M10). With a small dataset, even a high correlation coefficient may not reliably indicate a true underlying relationship. Such correlations are susceptible to overfitting and may not hold when applied to a larger set of compounds. Further, the observed trends should be interpreted as preliminary indications rather than definitive conclusions. Additional data points are necessary to confirm the robustness of these correlations and to identify potential outliers or nonlinear relationships. The mean unsigned deviation (MUSD) error values are also calculated for vibrational frequencies and ^{13}C NMR chemical shifts and are shown in Fig. S1. The overall MUSD error for vibrational frequency is 72.6 cm^{-1}. The NH stretching frequency is responsible for the large deviation. Similarly, the MUSD error of ^{13}C NMR chemical shift is 10.7 ppm.

http://dx.doi.org/10.29356/jmcs.v70i1.2378

J. Mex. Chem. Soc. **2026**, *70(1):e2378*
Regular Issue

ISSN-e 2594-0317

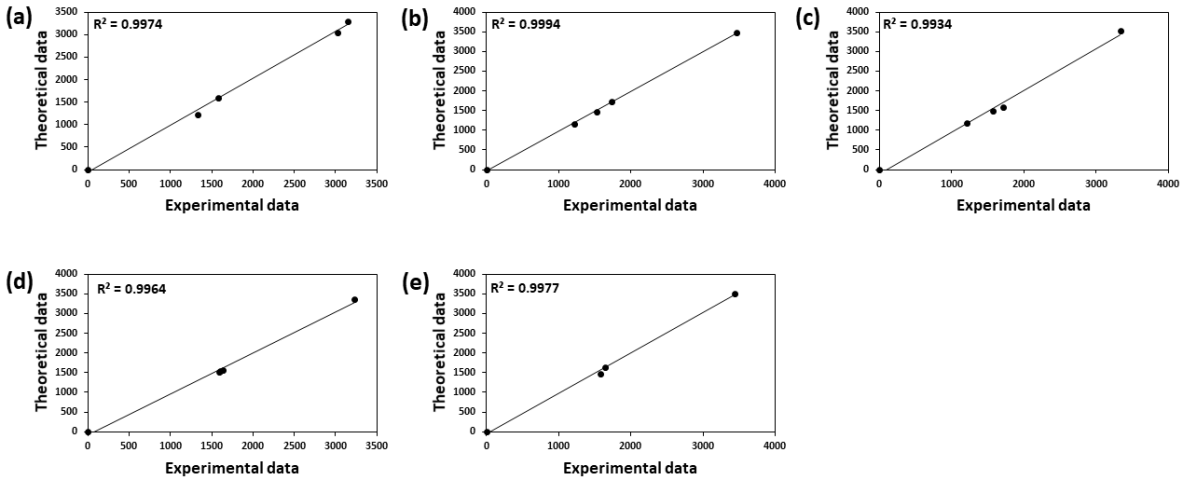

Fig. 3. Correlation studies of calculated and experimental IR vibrational frequencies of **(a)** M1, **(b)** M2, **(c)** M4, **(d)** M8, **(e)** M12 thiazole derivatives.

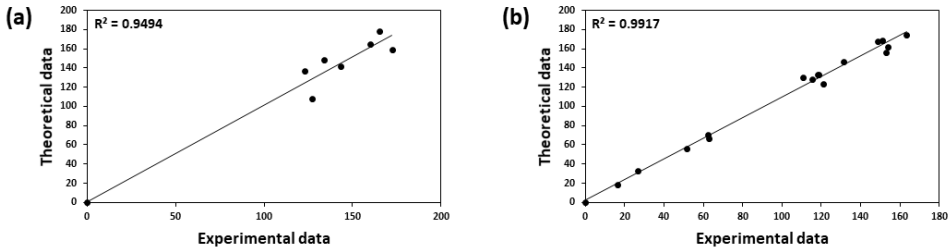

Fig. 4. Correlation studies of calculated and experimental ^{13}C NMR chemical shifts of (a) M1, (b) M10 thiazole derivatives.

Reactivity of thiazole-containing compounds

The frontier molecular orbital analysis is performed to obtain the DFT reactivity parameters of the selected thiazole-containing compounds. DFT reactivity parameters of the selected thiazole-containing compounds are given in Table 2. In particular, DFT parameters such as E_{HOMO}, E_{LUMO}, energy gap, ionization potential, electron affinity, chemical hardness, chemical potential, softness, electronegativity, and electrophilicity index are calculated using B3LYP/def2-TZVPP basis set. Table 2 shows that the energy gap value of selected thiazole-containing compounds varies from 2.13 eV (M1) to 4.52 eV (M4). This indicates that the M4 derivative is less reactive among the selected thiazole-containing compounds and M1 (2-(imino-4-nitrobenzol)-4-phenyl-5-(4-phenyl-1h-imidazol-2-yl)-thiazole) is highly reactive. M5 is the second highly reactive compound with an energy gap value of 3.26 eV. The energy gap values of the selected thiazole-containing compounds are in the order of M4 > M2 > M6 > M3 > M10 > M12 > M11 > M7 > M9 > M8 > M5 > M1. The positive HOMO and LUMO energy values are connected to the ionization energy and electron affinity of the system, respectively. Further, our calculated ionization energy values indicate that the selected thiazole-containing compounds have ionization energy values greater than 5 eV. Earlier studies have mentioned that organic compounds have higher ionization energy [50]. Our calculated results coincide well with this trend. Similarly, the electron affinity value of the selected thiazole-containing compounds varies from 1.08 eV (M6) to 3.06 eV (M1). The ability of the thiazole-containing compounds to absorb electrons is measured by the electrophilicity index, which is based on chemical potential and chemical hardness. Among the selected thiazole-containing compounds, the electrophilicity index value is low (2.44 eV) for M6 only. This indicates that M6 is less reactive than the other studied thiazole-containing

http://dx.doi.org/10.29356/jmcs.v70i1.2378

J. Mex. Chem. Soc. **2026**, *70(1):e2378*
Regular Issue

ISSN-e 2594-0317

compounds. This trend coincides well with the energy gap, ionization potential, and electron affinity values. Earlier Zhou et al. have mentioned that the compounds with lower global electrophilicity index are highly stable [51]. This trend coincides well with our calculated energy gap and chemical hardness values. Except M6 all other thiazole-containing compounds have electrophilicity where index value is greater than 3 eV.

In general, long-range electrostatic forces have a significant impact on the properties of biomolecules. These forces arise due to the presence of permanent electric dipole moments in the system. In the case of proteins, the particular arrangements of atoms will induce a strong electric field. This is the reason for secondary structures such as α-helix and β-sheet possess large macro-dipoles. The calculated dipole moment of the selected thiazole-containing compounds is given in Table 2. From Table 2, it can be seen that the calculated dipole moment value varies from 0.726 D (M12) to 7.484 D (M2). Further M1 is also having a higher dipole moment (7.059 eV). This indicates that these two thiazole-containing compounds (M1 and M2) are highly polar than the other selected thiazole-containing compounds. They are favorable for the formation of hydrogen bond interaction with the environment (water). As mentioned earlier, M1 possesses imidazole, $-NO_2$, amino and carboxylic groups. These functional groups are favorable for the non-covalent interactions in particular hydrogen bond interactions. Further, M1 possesses electronegative sites like N or O, and they are favorable for the formation of hydrogen bond interactions with the environment. The calculated energy gap values indicate that M1 and M5 are the first two highly reactive compounds. However, the dipole moment values indicate that the M5 has a lesser dipole moment (1.458 D). This shows that M5 is less stable in the liquid phase. Similarly, M2 has a higher dipole moment, and the energy gap value indicates that M2 is less reactive than M1. The claim regarding M1's stability in the liquid phase is supported by the combination of its larger dipole moment and lesser energy gap, favorable hydrogen bonding capability, and the polar nature of its functional groups. These features enhance its solvation and interaction with surrounding water molecules, leading to higher stability. This observation warrants further experimental validation to explore the solvation dynamics and its impact on the biological activity of M1. The high reactivity of M1, as suggested by its low energy gap (2.13 eV) and high electrophilicity index (Table 2), allows it to engage effectively in chemical interactions such as hydrogen bonding and π-stacking with protein targets. These characteristics are vital for its biological activity, as demonstrated by its strong binding affinity in docking studies. While high reactivity often implies instability, M1's structural design allows it to achieve a balance: its functional groups provide both the reactive sites needed for biological activity and the polar characteristics required for physical stability in aqueous environments. The dipole moment values of the selected thiazole-containing compounds are in the order of M2 > M1 > M4 > M11 > M7 > M10 > M6 > M8 > M9 > M5 > M3 > M12. Overall, M1 shows higher reactivity and stability in the liquid phase.

Table 2. Calculated HOMO, LUMO energies (eV), energy gap (eV), ionization potential (I in eV), electron affinity (A in eV), chemical hardness (η in eV), chemical potential (μ in eV), Softness (S in eV), electronegativity (χ in eV), electrophilicity index (ω), dipole moment (μ_M in D) of selected thiazole derivatives and standard drugs using B3LYP/def2-TZVPP.

Ligands	Pubchem ID	E_{HOMO}	E_{LUMO}	E_g	I	A	η	μ	S	χ	ω	μ_M
M1	168430219[a]	-5.1900	-3.0593	2.13	5.19	3.06	1.07	-4.12	0.46	4.12	7.98	7.059
M2	169452332[b]	-6.6733	-2.1973	4.48	6.67	2.20	2.24	-4.44	0.22	4.44	4.39	7.484
M3	168654967[c]	-6.0664	-1.7596	4.31	6.07	1.76	2.15	-3.91	0.23	3.91	3.56	1.258
M4	169452329[b]	-6.6776	-2.1543	4.52	6.67	2.15	2.26	-4.41	0.22	4.41	4.31	6.695
M5	168356046[d]	-5.8408	-2.5848	3.26	5.84	2.58	1.63	-4.21	0.30	4.21	5.45	1.458
M6	168301785[e]	-5.4141	-1.0825	4.33	5.41	1.08	2.17	-3.25	0.23	3.25	2.44	3.070
M7	168069291[f]	-5.3710	-1.5986	3.77	5.37	1.60	1.89	-3.48	0.26	3.48	3.22	3.735
M8	167530491[g]	-5.2750	-1.9613	3.31	5.28	1.96	1.66	-3.62	0.30	3.62	3.95	2.665

http://dx.doi.org/10.29356/jmcs.v70i1.2378

J. Mex. Chem. Soc. **2026**, *70(1):e2378*
Regular Issue

ISSN-e 2594-0317

Ligands	Pubchem ID	E_{HOMO}	E_{LUMO}	E_g	I	A	η	μ	S	χ	ω	μ_M
M9	168007999[h]	-5.7213	-2.2304	3.49	5.72	2.23	1.75	-3.98	0.28	3.98	4.53	2.393
M10	168008132[i]	-5.9920	-1.7677	4.22	5.99	1.77	2.11	-3.88	0.23	3.88	3.56	3.727
M11	168069315[f]	-5.5566	-1.7417	3.81	5.55	1.74	1.90	-3.64	0.26	3.64	3.49	4.773
M12	168300714[j]	-6.1746	-2.3011	3.87	6.17	2.30	1.94	-4.24	0.25	4.24	4.64	0.726

[a][35], [b][64], [c][65], [d][66], [e][67]. [f][68], [g][69], [70], [i][71], [j][72].

Physicochemical and pharmacokinetic properties

To identify whether a selected compound satisfies the Lipinski and Veber rule, the physicochemical properties of thiazole-containing compounds (1–12) must be investigated. Lipinski's rule of five, a substance must have the following requirements for bioavailability (a) molecular weight (MW) <500 g/mol or less; (b) the number of Hydrogen bond acceptors (nHBA) be no more than 10, (c) the number of hydrogen bond donors (nHBD) contain no more than 5 (d) octanol-water partition coefficient (log P) below 5. Furthermore, Veber rules are (a) Topological polar surface area (TPSA) must be less than or equal to 140 $Å^2$ and (b) the number of rotatable bonds (nrotb) must be less than 10. In this study, the ADMETLAB tool is used to determine the compliance of compounds (1–12) with the Lipinski and Veber rules. Further, the molinspiration web tool is used to calculate nRB and no. of violations. Our physicochemical studies indicate that the thiazole-containing compounds (1–12) are found to comply with the limits specified by Lipinski and Veber guidelines (Table 3) except M7, and M11. But these cases have one violation only. This shows that all the selected thiazole-containing compounds possess drug-likeness properties.

P-glycoprotein (P-gp) can act as membrane transporters for drug candidates in the extracellular or intracellular directions [52]. It plays an important role in protecting cells against drugs and toxins. P-gp is expressed in brain endothelial capillaries having the blood-brain barrier (BBB) to understand distribution. The drug candidates must have a molecular weight greater than 400 g/mol and a log P value greater than 4. Then P-gp can transport the drug (Table 3). In the present study, except M3, M5, M6, M7, M8, M9 and M12 all other ligands are estimated to be nontoxic and appropriate. Our studies indicate only M1 satisfies the above criteria, *i.e.* except M1 all other compounds cannot act as substrates of P-gp.

Table 3. The physicochemical properties and lipophilicity of the selected thiazole derivatives calculated using the ADMETLAB web tool.

Ligands	MW (g/mol)	nHBD	nHBA	nRB[a]	CLogp	TPSA	No. of violations[a]
M1	453.13	3	7	5	4.934	110.73	0
M2	487.89	1	5	3	3.259	71.0	0
M3	228.05	1	4	2	3.259	54.46	0
M4	443.94	1	5	4	4.911	67.77	0
M5	302.04	2	6	4	2.57	92.28	0
M6	241.02	1	1	0	0.282	12.03	0
M7	344.11	1	4	4	5.000	53.93	1

J. Mex. Chem. Soc. **2026**, *70(1):e2378*
Regular Issue

ISSN-e 2594-0317

Ligands	MW (g/mol)	nHBD	nHBA	nRB[a]	CLogp	TPSA	No. of violations[a]
M8	305.10	1	3	5	4.872	40.51	0
M9	305.94	0	2	2	4.169	25.78	0
M10	409.07	0	7	9	3.198	87.86	0
M11	518.0	1	4	5	7.269	50.7	2
M12	305.06	1	4	3	4.315	58.64	0
	<500	<5	<10	≤10[b]	<5		0

[a]Calculated using Molinspiration web tool, [b]Veber rule

In general, developing a drug is costly and time-consuming. To develop a drug, it is crucial to assess the pharmacokinetic features, including ADMET properties. In this study, the ADMETLAB tool is used to calculate the ADMET properties of all selected thiazole-containing compounds (1–12). Several ADMET characteristics are calculated for these selected compounds and are given in Table 4. These include human intestinal absorption (HIA), blood-brain barrier (BBB) penetration, plasma protein binding (PPB), cytochrome P450 enzymes (CYP1A2, CYP2C19, CYP2C9, CYP2D6, CYP3A4) inhibition, hERG inhibition, and synthetic accessibility (SA) score. The BBB is the microvascular endothelial cell layer of the brain, which acts as a barrier between the brain and blood. High BBB penetration is >2, medium absorption from 2 to 0.1, and low absorption is <0.1 [53]. This score indicates that all the selected thiazole-containing compounds (1–12) satisfy the ADMET requirements (see Table 4). Our study revealed that most of the thiazole-containing compounds considered in this study have BBB penetration values ranging from 0.0 to 0.8. This indicates that the selected thiazole-containing compounds have minimum potential for brain absorption. The potential risk of hERG activity inhibitors (pIC50) range is between 5.5 and 6.0 [54]. Our selected thiazole-containing compounds have pIC50 values well below this range. The synthetic accessibility score is 1 (simple) to 10 (difficult) [54]. Thiazole-containing compounds have an SA score between 2.603 (M5) and 5.828 (M6).

Table 4. The pharmacokinetic parameters of the selected thiazole derivatives.

Ligands	HIA	BBB Permeant	PPB	CYP1A2 inhibitor	CYP2C19 inhibitor	CYP2C9 inhibitor	CYP2D6 inhibitor	CYP3A4 inhibitor	hERG_pIC50	Synthetic accessibility score
M1	0.006	0.189	100.69%	0.814	0.937	0.954	0.445	0.436	0.930	2.769
M2	0.056	0.170	98.69%	0.966	0.865	0.924	0.440	0.398	0.988	3.093
M3	0.056	0.606	93.47%	0.987	0.851	0.622	0.524	0.099	0.970	2.640
M4	0.004	0.084	99.73%	0.908	0.906	0.780	0.146	0.502	0.959	3.097
M5	0.075	0.166	97.42%	0.697	0.206	0.246	0.037	0.051	0.998	2.603
M6	0.008	0.792	93.97%	0.888	0.785	0.488	0.818	0.582	0.873	5.828
M7	0.004	0.544	97.54%	0.977	0.886	0.923	0.938	0.807	0.964	2.783

http://dx.doi.org/10.29356/jmcs.v70i1.2378

J. Mex. Chem. Soc. **2026**, *70(1):e2378*
Regular Issue

ISSN-e 2594-0317

Ligands	HIA	BBB Permeant	PPB	CYP1A2 inhibitor	CYP2C19 inhibitor	CYP2C9 inhibitor	CYP2D6 inhibitor	CYP3A4 inhibitor	hERG_pIC50	Synthetic accessibility score
M8	0.012	0.784	95.42%	0.990	0.963	0.946	0.631	0.473	0.912	2.914
M9	0.010	0.025	99.43%	0.994	0.948	0.637	0.736	0.821	0.995	3.157
M10	0.003	0.076	99.05%	0.921	0.844	0.880	0.041	0.588	0.949	2.883
M11	0.003	0.078	101.7%	0.863	0.520	0.135	0.042	0.116	0.964	2.783
M12	0.125	0.209	98.36%	0.986	0.936	0.888	0.614	0.812	0.980	2.625

Molecular docking study

In order to evaluate the biological activity such as the antibacterial, anticancer, anticholinergic, and antifungal activity of the selected thiazole-containing compounds the molecular docking study is performed. The calculated binding energy values are given in Table 5. In the present study, it is performed to find out the lead compound among the ligands considered in this study.

Table 5. Molecular docking free binding energies (in kcal/mol) of selected ligands to various protein targets.

Ligands	Antibacterial activity					Anticancer activity		Anticholinergic activity		Antifungal activity	
	1KZN	4QGG	1DDE	3KR6	2Q85	1M17	1T46	4EY7	4BDS	1S16	5V5Z
M1	-9.1	-9.4	-8.7	-10.2	-11.3	-10.3	-9.8	-10.8	-11.6	-9.7	-11.6
M2	-8.6	-8.2	-7.9	-10.2	-9.1	-9.6	-9.4	-9.3	-10.0	-10.0	-9.7
M3	-7.5	-6.9	-7.1	-7.6	-7.6	-7.8	-8.4	-9.2	-9.1	-7.6	-8.4
M4	-7.7	-7.7	-8.2	-10.3	-9.5	-9.4	-9.0	-9.3	-9.2	-10.0	-10.2
M5	-8.1	-7.4	-7.0	-8.1	-8.2	-7.8	-8.7	-8.8	-9.1	-7.6	-8.2
M6	-6.3	-5.1	-5.2	-5.8	-6.2	-6.0	-7.0	-6.5	-6.2	-4.9	-6.3
M7	-8.5	-7.6	-8.1	-9.1	-8.7	-9.5	-8.9	-10.6	-9.0	-9.0	-9.5
M8	-7.3	-6.9	-7.3	-8.1	-8.5	-8.1	-9.0	-10.9	-8.3	-7.7	-9.5
M9	-6.7	-6.9	-5.6	-6.4	-6.9	-6.7	-6.0	-6.7	-7.1	-6.7	-6.4
M10	-6.9	-6.5	-6.3	-8.3	-7.9	-7.3	-7.2	-7.2	-8.5	-6.3	-7.2
M11	-9.0	-9.1	-8.1	-10.1	-9.9	-10.8	-10.1	-11.0	-10.6	-10.6	-11.0
M12	-8.1	-8.6	-8.1	-9.6	-8.6	-9.0	-9.8	-9.4	-10.2	-8.9	-9.2

http://dx.doi.org/10.29356/jmcs.v70i1.2378

J. Mex. Chem. Soc. **2026**, *70(1):e2378*
Regular Issue

ISSN-e 2594-0317

Antibacterial activity

To investigate the antibacterial activity of the selected thiazole-containing compounds. Few bacterial protein targets are identified and performed molecular docking studies on selected thiazole-containing compounds towards those protein targets. Earlier studies have mentioned that the thiazole-containing compounds possess antibacterial activity. The micro-dilution method is used to investigate the antibacterial activity experimentally. It can be used to determine the minimal bactericidal concentrations (MBC) and minimal inhibitory (MIC). The major role of the antibacterial agents are, affecting energy metabolism, destroying the integrity of cell membranes and cell walls, and inhibiting nucleic acid synthesis in bacteria. Hence, the chosen enzymes which are responsible for the above mechanisms are *E. Coli* gyrase (PDB ID: 1KZN), Thymidylate Kinase (PDB ID: 4QGG), *E. coli* Primase (PDB ID: 1DDE), *E. coli* MurA (PDB ID: 3KR6), *E. coli* MurB (PDB ID: 2Q85) for our antibacterial activity molecular docking study. The low binding energy means a strong interaction of the ligand to the enzyme. Our molecular docking study indicates that M1 has a lower binding energy value than other selected ligands (Table 5). M11 has the second lowest free energy. Among the selected protein targets, M1 has a lower value towards *E. coli* MurB (-11.3 kcal/mol). From Table 5, it can be noted that the inhibition of *E. coli* MurB is the suitable mechanism among the selected mechanisms with lower free energy of binding than the other mechanisms. This trend coincides very well with the earlier study by Kartsev et al [55]. Earlier, Kartsev et al have synthesized and studied the antimicrobial activity of new heteroaryl(aryl) thiazole-containing compounds. They have also performed molecular docking studies to investigate the antibacterial activity of those thiazole-containing compounds.

The docking pose of the most active ligand M1 to *E. coli* MurB shows four conventional hydrogen bond interactions. The amino acid residues such as GLU48, GLY49, SER50, and ASN51 residues form hydrogen bond interactions with the carboxylic group in the M1 ligand. Further, ASN51 also forms hydrogen bond interaction with the amino group attached to the benzene ring. Earlier, Babajan et al identified two catalytic domains (sequence from 33 to 168, from 228 to 362) in 2Q85 [56]. Our study shows M1 binds (-11.3 kcal/mol) in catalytic domain sequence from 33 to 168. However, the second domain plays a major role in the peptidoglycan biosynthesis [57]. The docked ligand M1 has a non-negligible affinity with 2Q85 which indicates that it possesses antibacterial activity. The ligand M1 also shows good binding affinity (-10.2 kal/mol) with MurA. The MurA plays an important role in the catalysis of peptidoglycan biosynthesis, and it is a suitable target for antibacterial activity. Multiple conventional hydrogen bond interactions take place between M1 and 3KR6 (Fig. 5). ARG331, ARG371, and CYS115 form hydrogen bond interactions with the carboxylic group in the M1 ligand. ASN23 forms a hydrogen bond with an amino group attached to the benzene ring.

The molecular docking results reveal several key interactions between the selected ligands and target proteins, particularly for the highly reactive compound M1. For example, ARG120 forms a hydrogen bond with the sulfur atom in the thiazole group, and SER162 interacts via hydrogen bonding with the amino group in the imidazole ring. These interactions confirm that M1 binds effectively within the active region of 3KR6, as described in earlier studies by Frlan et al [58]. The high reactivity of M1, indicated by its low energy gap (2.13 eV) and high electrophilicity index, provides a molecular basis for its strong binding affinity and interaction capability. The sulfur atom in the thiazole ring, being part of the π-electron system, is more likely to participate in hydrogen bonding due to the enhanced nucleophilic character, as predicted by the frontier molecular orbital analysis. Similarly, the amino group in the imidazole ring, known for its electron-donating ability, facilitates hydrogen bond formation, further stabilizing the ligand-protein complex. The electrophilic nature of M1, as reflected by its high electrophilicity index, makes it an excellent candidate for forming hydrogen bonds with amino acid residues, such as ARG120 and SER162. These interactions are crucial for stabilizing the ligand-protein complex. The high dipole moment of M1 (7.059 D) suggests its strong interaction with polar residues in the protein, further enhancing its binding affinity. This is evident in its ability to form polar interactions, such as the hydrogen bonds with ARG120 and SER162. These results highlight the significant role of reactivity in interpreting and rationalizing the docking interactions. The strong correlation between the computational reactivity parameters and the docking results strengthens the reliability of the findings and the predictive power of density functional theory in studying bioactive compounds.

http://dx.doi.org/10.29356/jmcs.v70i1.2378

J. Mex. Chem. Soc. **2026**, *70(1):e2378*
Regular Issue

ISSN-e 2594-0317

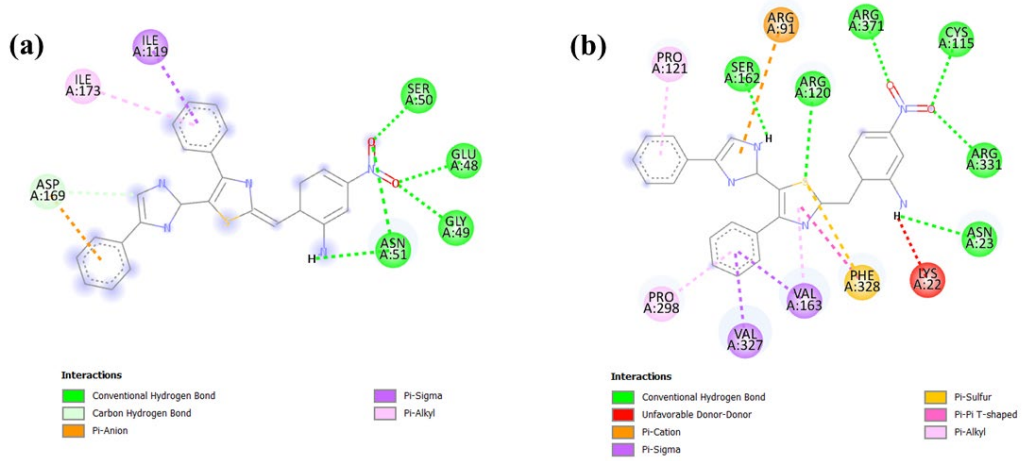

Fig. 5. Binding interactions of **(a)** M1 with 2Q85, **(b)** M1 with 3KR6.

Anticancer activity

The thiazole-containing compounds have remarkable binding affinity against numerous protein targets which play a vital role in cancer cell growth. Among the targets, epidermal growth factor receptor (EGFR) kinase and tyrosine kinase (TRK) are significant oncology targets. This is due to their important role in the unusual cancer cell signaling. Further, EGFR overexpression has been observed in many solid tumors, for example, colon cancer, ovarian cancer, head and neck cancer, etc. It must be noted that dasatinib and dabrafenib are thiazole-based drugs that show inhibitory activity against tyrosine kinase. Hence, it is interesting to study the anticancer potential of the selected ligands against these kinases. In general, chemotherapy is a major technique used for localized and metastasized cancer. Therefore, in vitro cytotoxicity and growth inhibitory activity against the human tumor cell lines for various cancers were investigated experimentally. The anticancer activity of the selected thiazole-containing compounds is evaluated in the active site of these kinases using the molecular docking technique. The crystal structure of EGFR kinase (1M17) and tyrosine kinase (1T46) are taken from the protein data bank. The docking results are given in Table 5 and shown in Fig. 6. From Table 5, it can be seen that M1 and M11 have lower binding energy values than other selected ligands. Among 1M17 and 1T46, these ligands show lower values in 1M17. This indicates that these ligands have strong binding with EGFR than TRK. Our calculated binding energy values coincide with the earlier study by Jain et al [59]. They have studied Schiff-based thiazole ligands and their complexes. They found that the lower binding energy of their compounds is -9.63, and -10.40 kcal/mol for 1M17 and 1T46 respectively.

The catalytic domain of EGFR consists of LEU764, LEU694, GLN767, LEU768, ALA719, THR766, PRO770, MET769, GLY772, PHE771, THR830, ASP831, and LEU820 residues [60]. From Fig. 6, it can be confirmed that the ligand M1 binds in the active region of EGFR kinase. Multiple conventional hydrogen bonds are observed between M1 and EGFR kinase. That is, hydrogen bond interaction takes place between ARG817 with the carboxylic group in M1, ASN818, and ASP831 with the amino group attached to the benzene ring. ASP831 forms another hydrogen bond interaction with the amino group in the thiazole ring. These multiple hydrogen bond interactions could be the reason for the higher binding affinity of M1 with EGFR kinase. In general, binding energy and a number of hydrogen bonds are used to rank the best binding ligands.

J. Mex. Chem. Soc. **2026**, *70(1):e2378*
Regular Issue

ISSN-e 2594-0317

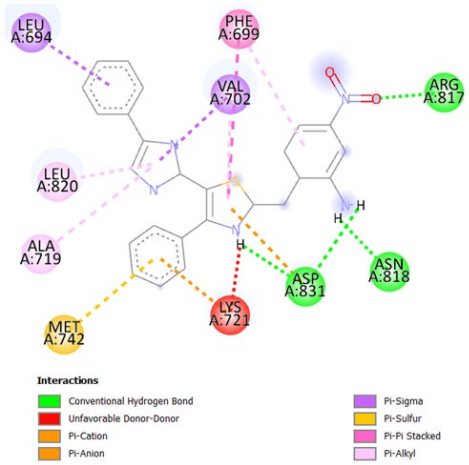

Fig. 6. Binding interactions of M1 with EGFR (1M17).

Anticholinergic activity

To investigate the anticholinergic activity, molecular docking studies are performed on cholinesterase (4EY7 and 4BDS) with the selected thiazole-containing compounds. The binding energies are given in Table 5. Among the selected thiazole-containing compounds, M1 has strong binding (-11.6 kcal/mol) with 4BDS. This is in consistent with the previous study by Mughal et al., [61]. They have investigated the potential anticholinergic inhibition activity of flavonols. Fig. 7 shows the binding interactions of M1 with 4BDS. The M1 ligand shows its inhibitory activity (carboxylic group attached with a benzene ring) inside the catalytic active region of BChE by forming conventional hydrogen bonding interaction with TYR128 and SER198 of 4BDS. Similarly, HIS438 forms a hydrogen bond interaction with the amino group attached to the benzene ring. Another hydrogen bond interaction takes place between PRO285 and with imidazole ring in M1. Apart from this, few hydrophobic interactions take place between TRP231 and the benzene ring as well as LEU286 with the benzene ring. Our calculated results indicate that the binding interaction is active. Similarly, all the selected ligands have strong interaction with 4BDS. A similar trend is noted in the previous study by Mughal et al. They have performed a molecular docking study on the standard drug with 4BDS. Their calculated binding energy value is -6.8 kcal/mol. Our calculated binding energy value of the M1 ligand is lower than (-11.6 kcal/mol) their reported standard drug THA (Tarenflurbil) theoretical value. This indicates that the M1 ligand is more active than the standard drug. However, it is necessary to perform an experimental study to validate this hypothesis.

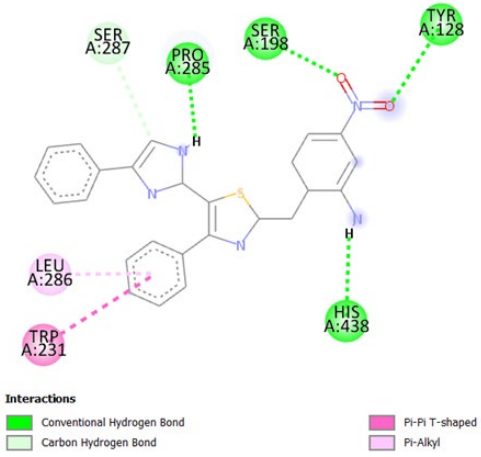

Fig. 7. Binding interactions of M1 with 4BDS.

http://dx.doi.org/10.29356/jmcs.v70i1.2378

J. Mex. Chem. Soc. **2026**, *70(1):e2378*
Regular Issue

ISSN-e 2594-0317

Antifungal activity

In general, the micro-dilution method is used to understand the antifungal activity of the synthesized compounds experimentally. By using the molecular docking technique one can theoretically understand the antifungal activity. Earlier Kartsev et al. studied the antifungal activity of their synthesized compounds [55]. They have also performed molecular docking studies to understand their antifungal activity. They have used ketoconazole a standard drug for comparison purposes. To investigate the antifungal activity of the selected thiazole-containing compounds, the selected ligands are docked with DNA topoisomerase IV and lanosterol 14α-demethylase of *C-albicans*. Our calculated binding energies are given in Table 5. Our calculations show that the M1 ligand has a strong binding affinity (-11.6 kcal/mol) with 5V5Z (Fig. 8). All other ligands have lesser binding energy than the M1 ligand. Our calculated binding energy values are comparably lower than the earlier study by Kartsev et al. They found that their compound 9 has a lower energy value (-9.21 kcal/mol). They also found that the ketoconazole has a binding energy value of -8.23 kcal/mol. In the present study, most of the selected ligands have lower binding energy than ketoconazole except M5, M6, M9, and M10.

Fig. 8 shows the binding interactions of M1 with 5V5Z. It is interesting to see that there is no conventional hydrogen bond interaction takes place between M1 and amino acid residues in 5V5Z. There are plenty of hydrophobic interactions that take place between M1 and 5V5Z. Most of the hydrophobic interactions such as π-σ, π-sulfur, and π-alkyl take place between benzene rings in M1 and amino acid residues. Earlier Kartsev et al. found that TYR64, TYR118, and TYR132 residues are involved in hydrogen bonding interactions. In our study, TYR118 and TYR132 form hydrophobic π-alkyl interaction with the benzene ring in M1. This is in contrast to our antibacterial and anticancer activity docking studies. In those cases, hydrogen bond interaction takes place in the carboxylic group and amino group attached to the benzene ring in the M1 ligand. No such hydrogen bond interaction exists between M1 and 5V5Z.

The reactivity analysis, based on parameters such as energy gap, electrophilicity index, and dipole moment, provides the foundation for understanding the molecular interactions observed in docking studies. The high reactivity of M1, as indicated by its low energy gap (2.13 eV), correlates with its strong binding affinity to multiple protein targets. The electrophilic regions of M1, such as the sulfur in the thiazole ring and the nitro group, align with the hydrogen bonding interactions observed in docking studies (e.g., with ARG120 and SER162 in 3KR6). These interactions are critical for the ligand's stability and specificity in the binding pocket.

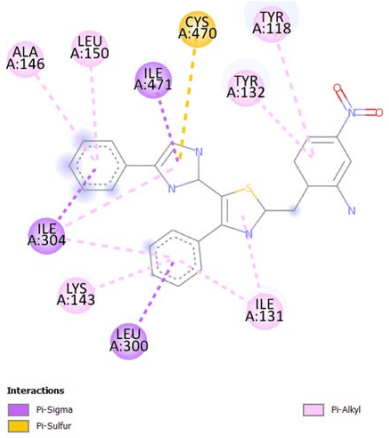

Fig. 8. Binding interactions of M1 with 5V5Z.

Molecular dynamics simulation

In general, to understand the structural stability and interaction between protein and ligand, molecular dynamics simulations are performed. In the present study, MD simulation is performed on protein 1M17 as well as a protein-ligand complex of 1M17 protein with M1 over 20 ns. The reason for the selection of 1M17 protein for the MD study is, as mentioned earlier EGFR kinase is a significant oncology target because of its important role in the abnormal signaling of cancer cells. Further, MD simulations are performed to demonstrate the binding affinity of the M1 ligand with 1M17 protein. Our docking study revealed that M1 has better binding energy with the selected protein

J. Mex. Chem. Soc. **2026**, *70(1):e2378*
Regular Issue

ISSN-e 2594-0317

targets. Statistical analysis techniques such as RMSD, RMSF, Radius of gyration, and number of hydrogen bonds are used to study the structural stability and binding affinity of the selected protein-ligand complex. To complement the textual analysis, the 3D structure of the protein-ligand complex, focusing on the binding zone, is included (Fig. 9). A close-up view of the binding region of the M1-1M17 complex can showcase the specific residues involved (e.g., PHE699, MET742, ASP831, ASN818, ARG817, LEU820) and their interactions with M1. These visuals can help readers understand the structural basis for the observed stability in the simulation.

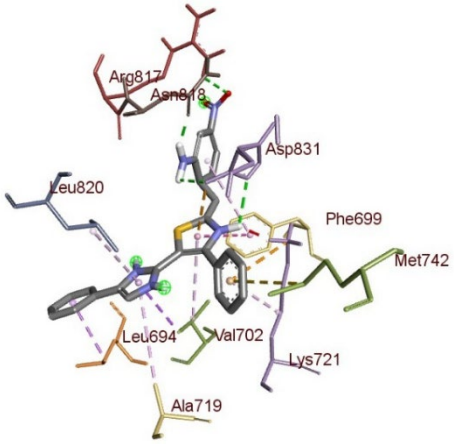

Fig. 9. 3D plot of binding region of M1-1M17 complex.

RMSD is used to understand the conformational changes from the original structure during the simulation time. The RMSD is for measuring the degree of fluctuation of the protein backbone when drug compounds are docked in it. RMSD of the selected 1M17-M1 complex is performed for 20 ns and is shown in Fig. 10, along with the RMSD of 1M17. From Fig. 10, it can be seen that the RMSD value is high (~10 Å) in both the cases of 1M17 and 1M17-M1 complex. A large structural deviation is noted in the initial simulation period. That is up to upto10 ns, large structural changes are noted, and after that, it is stabilized. The reason for the large deviation from the initial structure is, 1M17 has 15 α-helix structures and 11 β-sheet structures. After TYR867, no intramolecular β-sheet structure and after TYR954 no secondary structure is noted up to ASP988 residue. This large polypeptide chain caused large structural changes during the simulation due to the floppiness in the main chain of the amino acid residues. A similar trend is observed in both the 1M17 and 1M17-M1 complex during the MD simulation. However, the 1M17 as well as 1M17-M1 complex is stabilized after 10 ns, which shows that the M1 and 1M17 bind strongly and maintain their overall shape.

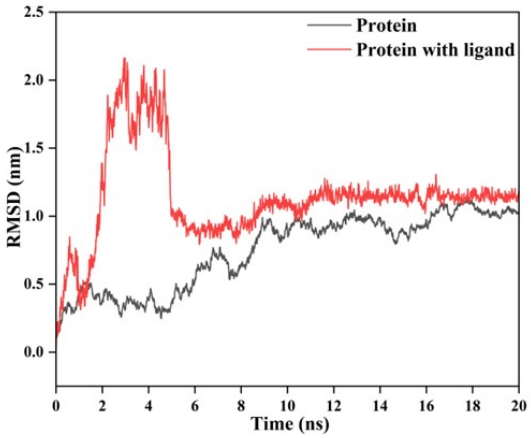

Fig. 10. RMSD calculation of protein (1M17) and protein (1M17) with ligand (M1) during 20 ns molecular dynamics simulation.

http://dx.doi.org/10.29356/jmcs.v70i1.2378

J. Mex. Chem. Soc. **2026**, *70(1):e2378*
Regular Issue

ISSN-e 2594-0317

To get deeper insights into the structural fluctuation in protein and protein-ligand complex RMSF is calculated in this study. RMSF is a measure of the mean deviation of atoms from their equilibrium position. The RMSF value is calculated for the 1M17 and 1M17-M1 complex and is shown in Fig. 11. In general, the RMSF value is higher in C- and N-terminal regions. Because they have more freedom to move at the end of the polypeptide chain, like terminal blockers in a peptide chain [62]. A similar trend is noted in the RMSF value of 1M17 and 1M17-M1 complex. From Fig. 11, it can be seen that, after the atom number 4000, a large fluctuation is noted in both cases. This indicates that the fluctuation arises due to the terminal residues in the 1M17 protein. This is in agreement with the RMSD result. Apart from this, the RMSF value of other atoms ranges from 0.1 to 0.5 nm which shows that the protein and ligand are relatively stable, because of the minor fluctuations in their atomic positions during the simulation.

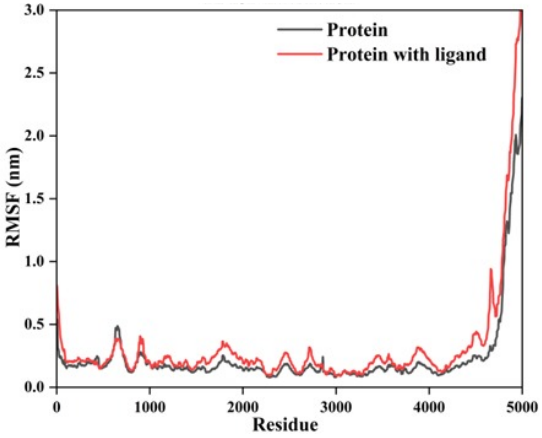

Fig. 11. RMSF calculation of protein (1M17) and protein (1M17) with ligand (M1) during 20 ns molecular dynamics simulation.

The Radius of gyration (R_g) is an indicator of the conformational changes of protein in MD simulation. In the present study, Rg values are used to study the interaction between the M1 ligand and 1M17 protein (Fig. 12). The R_g values for the 1M17-M1 complex and 1M17 are 2.19 and 2.18 nm, respectively. This similarity suggests that the M1 ligand does not induce major structural changes in the protein. In addition, our MD simulation shows the number of hydrogen bonds formed between protein (1M17) and ligand (M1) varies between 0 and 4 during the simulation period (Fig. 13). The formation of multiple hydrogen bonds indicates that the selected ligand M1 has the potential to bind with the active site of 1M17. However, it is necessary to perform further analysis to understand the importance of these hydrogen bonds in the biological activity of 1M17.

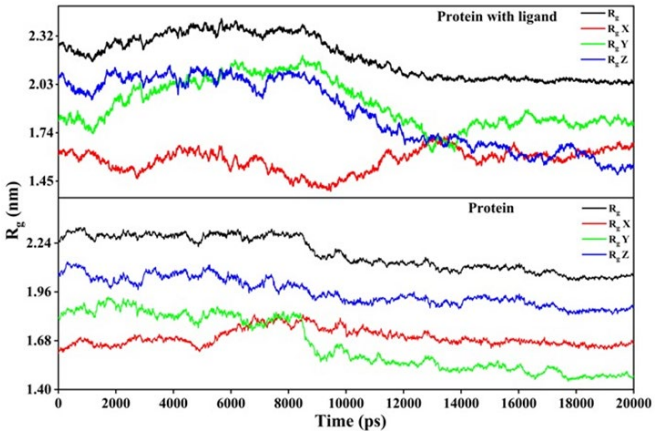

Fig. 12. Radius of gyration vs Time (in ps) plots of protein (1M17) and protein (1M17) with ligand (M1) during 20 ns molecular dynamics simulation.

http://dx.doi.org/10.29356/jmcs.v70i1.2378

J. Mex. Chem. Soc. **2026**, *70(1):e2378*
Regular Issue

ISSN-e 2594-0317

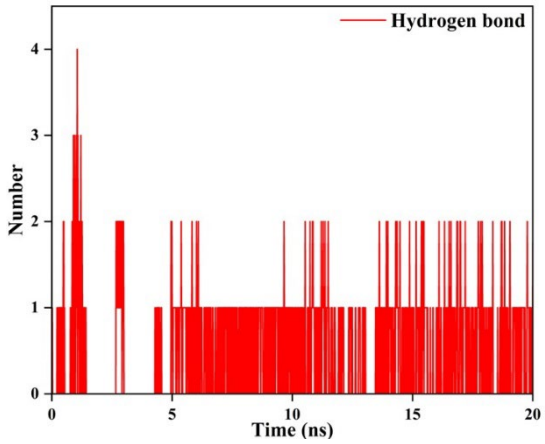

Fig. 13. No. of hydrogen bonds vs Time (in ps) plots of protein (1M17) and protein (1M17) with ligand (M1) during 20 ns molecular dynamics simulation.

The molecular dynamics simulations reinforce the trends observed in reactivity and docking studies by providing a dynamic view of ligand stability and binding. The RMSD and RMSF analyses show minimal fluctuations, indicating that M1 maintains its binding interactions throughout the simulation. The stability of interactions with residues like ASP831 and ARG817 in 1M17 suggests a strong correlation between M1's reactivity and its binding efficiency. The radius of gyration analysis shows that M1 binding does not induce significant structural changes in the protein, emphasizing the compatibility of the ligand's reactivity profile with the protein's binding site. The common thread across the reactivity, docking, and molecular dynamics studies is the role of electronic and structural properties in determining the biological activity of the thiazole derivatives.

In summary, our computational studies indicate that M1 possesses significant biological activity. Earlier Dekate et al. studied imidazole-thiazole hybrids using experimental and bioinformatics tools [34, 35]. They have investigated antibacterial and antifungal activity. They found that these hybrids possess significant antimicrobial activities. Our results coincide well with their study. Further, our computational studies revealed that M1 possesses anticancer and anticholinergic activity. This confirms that M1 has significant biological activity and could be useful for the development of medications against cancer and Alzheimer's disease.

Conclusions

In the present study, a few recently synthesized thiazole-containing compounds are investigated to understand their biological activity using various computational techniques. There are 12 thiazole-containing compounds are identified as bioactive compounds. Density functional theory calculations are performed on these 12 thiazole-containing compounds to study their structure and reactivity. The molecular geometry of the selected thiazole-containing compounds is optimized using B3LYP functional with a def2-TZVPP basis set. Our calculated structural parameters coincide well with the experimental data. This shows that B3LYP functional with def2-TZVPP basis set is suitable for studying these thiazole-containing compounds. Our DFT calculations revealed that M1 exhibits the highest reactivity, characterized by a low energy gap, high electrophilicity index, and a significant dipole moment. The structure-reactivity relationship demonstrates that functional groups such as nitro, imidazole, and thiazole are pivotal for enhancing reactivity and binding affinity. The docking studies confirm the strong binding affinity of M1 with various protein targets, with key interactions including hydrogen bonds and π-stacking. These interactions are consistent with the predicted electrophilic and nucleophilic sites identified in the reactivity analysis. MD simulations validate the dynamic stability of M1-protein complexes. The low fluctuations in RMSD and RMSF, along with stable hydrogen bond formation, reinforce the conclusion that M1 maintains its binding interactions throughout the simulation. The radius of

http://dx.doi.org/10.29356/jmcs.v70i1.2378

ISSN-e 2594-0317

gyration analysis further confirms that M1 binding does not induce significant conformational changes in the proteins, indicating strong compatibility. The combined results highlight M1 as a promising candidate for drug development due to its superior reactivity, strong protein binding interactions, and dynamic stability. Finally, this study presents a comprehensive computational investigation into the structure, reactivity, and biological activity of recently synthesized thiazole derivatives using density functional theory (DFT), molecular docking, and molecular dynamics (MD) simulations. The integration of these approaches provides a unified understanding of the potential applications of these compounds in drug development.

Acknowledgements

S.P. contributed to the calculations, formal analysis, investigations, original draft preparation, editing the manuscript, and supervision; S.G. contributed to the calculations, editing the manuscript, K.A. contributed to formal analysis and investigations, A.A. contributed to formal analysis and editing the manuscript. All authors read and approved the final manuscript.

References

1. Tripathi, A. C.; Gupta, S. J.; Fatima, G. N.; Sonar, P. K.; Verma, A.; Saraf, S. K. *Eur. J. Med. Chem.* **2014**, *72*, 52–77. DOI: https://doi.org/https://doi.org/10.1016/j.ejmech.2013.11.017
2. Kaminskyy, D.; Kryshchyshyn, A.; Lesyk, R. *Eur. J. Med. Chem.* **2017**, *140*, 542–594. DOI: https://doi.org/https://doi.org/10.1016/j.ejmech.2017.09.031
3. Kamble, R. D.; Meshram, R. J.; Hese, S. V.; More, R. A.; Kamble, S. S.; Gacche, R. N.; Dawane, B. S. *Comput. Biol. Chem.* **2016**, *61*, 86–96. DOI: https://doi.org/https://doi.org/10.1016/j.compbiolchem.2016.01.007
4. Mohareb, R.; Al-Omran, F.; Abdelaziz, M.; Ibrahim, R. *Acta Chim. Slov.* **2017**, *64*, 349–364.
5. Gümüş, M.; Yakan, M.; Koca, İ. *Future Med. Chem.* **2019**, *11*, 1979–1998. DOI: https://doi.org/10.4155/fmc-2018-0196
6. Bikobo, D. S. N.; Vodnar, D. C.; Stana, A.; Tiperciuc, B.; Nastasă, C.; Douchet, M.; Oniga, O. *J. Saudi Chem. Soc.* **2017**, *21*, 861–868. DOI: https://doi.org/https://doi.org/10.1016/j.jscs.2017.04.007
7. Althagafi, I.; El-Metwaly, N.; Farghaly, T. A. *Molecules.* **2019**, *24*, 1741. DOI: https://doi.org/10.3390/molecules24091741
8. Biernasiuk, A.; Kawczyńska, M.; Berecka-Rycerz, A.; Rosada, B.; Gumieniczek, A.; Malm, A.; Dzitko, K.; Łączkowski, K. Z. *Med. Chem. Res.* **2019**, *28*, 2023–2036. DOI: https://doi.org/10.1007/s00044-019-02433-2
9. Bondock, S.; Fouda, A. M. *Synth. Commun.* **2018**, *48*, 561–573. DOI: https://doi.org/10.1080/00397911.2017.1412465
10. Borcea, A. M.; Ionuț, I.; Crișan, O.; Oniga, O. *Molecules.* **2021**, *26*, 624. DOI: https://doi.org/10.3390/molecules26030624
11. Carbone, A.; Cascioferro, S.; Parrino, B.; Carbone, D.; Pecoraro, C.; Schillaci, D.; Cusimano, M. G.; Cirrincione, G.; Diana, P. *Molecules.* **2021**, *26*, 81. DOI: https://doi.org/10.3390/molecules26010081
12. Ayati, A.; Emami, S.; Moghimi, S.; Foroumadi, A. *Future Med. Chem.* **2019**, *11*, 1929–1952. DOI: https://doi.org/10.4155/fmc-2018-0416
13. Carbone, D.; Vestuto, V.; Ferraro, M. R.; Ciaglia, T.; Pecoraro, C.; Sommella, E.; Cascioferro, S.; Salviati, E.; Novi, S.; Tecce, M. F.; Amodio, G.; Iraci, N.; Cirrincione, G.; Campiglia, P.; Diana, P.; Bertamino, A.; Parrino, B.; Ostacolo, C. *Eur. J. Med. Chem.* **2022**, *234*, 114233. DOI: https://doi.org/10.1016/j.ejmech.2022.114233
14. Di Franco, S.; Parrino, B.; Gaggianesi, M.; Pantina, V. D.; Bianca, P.; Nicotra, A.; Mangiapane, L. R.; Lo Iacono, M.; Ganduscio, G.; Veschi, V.; Brancato, O. R.; Glaviano, A.; Turdo, A.; Pillitteri, I.; Colarossi, L.; Cascioferro, S.; Carbone, D.; Pecoraro, C.; Fiori, M. E.; De Maria, R.; Todaro, M.;

J. Mex. Chem. Soc. **2026**, *70(1):e2378*
Regular Issue

ISSN-e 2594-0317

Screpanti, I.; Cirrincione, G.; Diana, P.; Stassi, G. *iScience.* **2021**, *24*, 102664. DOI: https://doi.org/10.1016/j.isci.2021.102664
15. Muhammad, Z. A.; Masaret, G. S.; Amin, M. M.; Abdallah, M. A.; Farghaly, T. A. *Med. Chem.* **2017**, *13*, 226–238. DOI: http://dx.doi.org/10.2174/1573406412666160920091146
16. Kryshchyshyn, A.; Roman, O.; Lozynskyi, A.; Lesyk, R. *Sci. Pharm.* **2018**, *86*, 26. DOI: https://doi.org/10.3390/scipharm86020026
17. Petrou, A.; Eleftheriou, P.; Geronikaki, A.; Akrivou, M. G.; Vizirianakis, I. *Molecules.* **2019**, *24*, 3821. DOI: https://doi.org/10.3390/molecules24213821
18. Khatik, G. L.; Datusalia, A. K.; Ahsan, W.; Kaur, P.; Vyas, M.; Mittal, A.; Nayak, S. K. *Curr. Drug Discovery Technol.* **2018**, *15*, 163–177. DOI: https://doi.org/10.2174/1570163814666170915134018
19. Grozav, A.; Porumb, I. D.; Găină, L. I.; Filip, L.; Hanganu, D. *Molecules* **2017**, *22*, 260. DOI: https://doi.org/10.3390/molecules22020260
20. Djukic, M.; Fesatidou, M.; Xenikakis, I.; Geronikaki, A.; Angelova, V. T.; Savic, V.; Pasic, M.; Krilovic, B.; Djukic, D.; Gobeljic, B.; Pavlica, M.; Djuric, A.; Stanojevic, I.; Vojvodic, D.; Saso, L. *Chem.-Biol. Interact.* **2018**, *286*, 119–131. DOI: https://doi.org/10.1016/j.cbi.2018.03.013
21. Liaras, K.; Fesatidou, M.; Geronikaki, A. *Molecules.* **2018**, *23*, 685. DOI: https://doi.org/10.3390/molecules23030685
22. Jacob, P. J.; Manju, S. L. *Bioorg. Chem.* **2020**, *100*, 103882. DOI: https://doi.org/10.1016/j.bioorg.2020.103882
23. Brito, C. C. B.; da Silva, H. V. C.; Brondani, D. J.; de Faria, A. R.; Ximenes, R. M.; da Silva, I. M.; de Albuquerque, J. F. C.; Castilho, M. S. *J. Enzyme Inhib. Med. Chem.* **2019**, *34*, 573–584. DOI: https://doi.org/10.1080/14756366.2018.1550752
24. Rodrigues, C. A.; dos Santos, P. F.; da Costa, M. O. L.; Pavani, T. F. A.; Xander, P.; Geraldo, M. M.; Mengarda, A.; de Moraes, J.; Rando, D. G. G. *J. Venomous Anim. Toxins Incl. Trop. Dis.* **2018**, *24*, 31. DOI: https://doi.org/10.1186/s40409-018-0163-x
25. Rouf, A.; Tanyeli, C. *Eur. J. Med. Chem.* **2015**, *97*, 911–927. DOI: https://doi.org/10.1016/j.ejmech.2014.10.058
26. Hadziyannis, S. J.; Papatheodoridis, G. V. *Expert Rev. Anti-Infect. Ther.* **2004**, *2*, 475–483.
27. Pasqualotto, A. C.; Thiele, K. O.; Goldani, L. Z. *Curr. Opin. Invest. Drugs.* **2010**, *11*, 165–174.
28. Kardos, N.; Demain, A. L. *Appl. Microbiol. Biotechnol.* **2011**, *92*, 677–687. DOI: https://doi.org/10.1007/s00253-011-3587-6
29. Borelli, C.; Schaller, M.; Niewerth, M.; Nocker, K.; Baasner, B.; Berg, D.; Tiemann, R.; Tietjen, K.; Fugmann, B.; Lang-Fugmann, S.; Korting, H. C. *Chemotherapy.* **2008**, *54*, 245–259. DOI: https://doi.org/10.1159/000142334
30. Thierbach, G.; Reichenbach, H. *Antimicrob. Agents Chemother.* **1981**, *19*, 504–507. DOI: https://doi.org/10.1128/AAC.19.4.504
31. Li, X. H.; Yang, X. L.; Ling, Y.; Fan, Z. J.; Liang, X. M.; Wang, D. Q.; Chen, F. H.; Li, Z. M. *J. Agric. Food Chem.* **2005**, *53*, 2202–2206. DOI: https://doi.org/10.1021/jf0403944
32. Murray, C. J.; Ikuta, K. S.; Sharara, F.; Swetschinski, L.; Robles Aguilar, G.; Gray, A.; Han, C.; Bisignano, C.; Rao, P.; Wool, E.; Johnson, S. C.; Browne, A. J.; Chipeta, M. G.; Fell, F.; Hackett, S.; Haines-Woodhouse, G.; Kashef Hamadani, B. H.; Kumaran, E. A. P.; McManigal, B.; Agarwal, R.; Akech, S.; Albertson, S.; Amuasi, J.; Andrews, J.; Aravkin, A.; Ashley, E.; Bailey, F.; Baker, S.; Basnyat, B.; Bekker, A.; Bender, R.; Bethou, A.; Bielicki, J.; Boonkasidecha, S.; Bukosia, J.; Carvalheiro, C.; Castañeda-Orjuela, C.; Chansamouth, V.; Chaurasia, S.; Chiurchiù, S.; Chowdhury, F.; Cook, A. J.; Cooper, B.; Cressey, T. R.; Criollo-Mora, E.; Cunningham, M.; Darboe, S.; Day, N. P. J.; De Luca, M.; Dokova, K.; Dramowski, A.; Dunachie, S. J.; Eckmanns, T.; Eibach, D.; Emami, A.; Feasey, N.; Fisher-Pearson, N.; Forrest, K.; Garrett, D.; Gastmeier, A.; Giref, A. Z.; Greer, R. C.; Gupta, V.; Haller, S.; Haselbeck, A.; Hay, S. I.; Holm, M.; Hopkins, S.; Iregbu, K. C.; Jacobs, J.; Jarovsky, D.; Javanmardi, F.; Khorana, M.; Kissoon, N.; Kobeissi, E.; Kostyanev, T.; Krapp, F.; Krumkamp, R.; Kumar, A.; Kyu, H. H.; Lim, C.; Limmathurotsakul, D.; Loftus, M. J.; Lunn, M.; Ma, J.; Mturi, N.; Munera-Huertas, T.; Musicha, P.; Mussi-Pinhata, M. M.; Nakamura, T.; Nanavati, R.; Nangia, S.; Newton, P.; Ngoun, C.; Novotney, A.; Nwakanma, D.; Obiero, C. W.; Olivas-Martinez, A.; Olliaro, P.; Ooko, E.; Ortiz-Brizuela, E.; Peleg, A. Y.; Perrone, C.; Plakkal, N.; Ponce-de-Leon,

J. Mex. Chem. Soc. **2026**, *70(1):e2378*
Regular Issue

ISSN-e 2594-0317

A.; Raad, M.; Ramdin, T.; Riddell, A.; Roberts, T.; Robotham, J. V.; Roca, A.; Rudd, K. E.; Russell, N.; Schnall, J.; Scott, J. A. G.; Shivamallappa, M.; Sifuentes-Osornio, J.; Steenkeste, N.; Stewardson, A. J.; Stoeva, T.; Tasak, N.; Thaiprakong, A.; Thwaites, G.; Turner, C.; Turner, P.; van Doorn, H. R.; Velaphi, S.; Vongpradith, A.; Vu, H.; Walsh, T.; Waner, S.; Wangrangsimakul, T.; Wozniak, T.; Zheng, P.; Sartorius, B.; Lopez, A. D.; Stergachis, A.; Moore, C.; Dolecek, C.; Naghavi, M. *Lancet.* **2022**, *399*, 629–655. DOI: https://doi.org/10.1016/S0140-6736(21)02724-0

33. Jonas, O. B.; Irwin, A.; Berthe, F. C. J.; Le Gall, F. G.; Marquez, P. V. *World Bank Rep.* **2017**, *2*.
34. Nikalje, A. P. G.; Tiwari, S. V.; Sarkate, A. P.; Karnik, K. S. *Med. Chem. Res.* **2018**, *27*, 157–169. DOI: https://doi.org/10.1007/s00044-017-2085-5
35. Dekate, S. M.; Hatzade, K. M.; Ghatole, A. M. *Iran. J. Sci.* **2023**, *47*, 953–961. DOI: https://doi.org/10.1007/s40995-023-01496-6
36. Grob, S. Molinspiration Cheminformatics Free Web Services. **2022**. https://www.molinspiration.com/, accessed in May 2024.
37. Kim, S.; Chen, J.; Cheng, T.; Gindulyte, A.; He, J.; He, S.; Li, Q.; Shoemaker, B. A.; Thiessen, P. A.; Yu, B.; Zaslavsky, L.; Zhang, J.; Bolton, E. E. *Nucleic Acids Res.* **2023**, *51*, D1373–D1380. DOI: https://doi.org/10.1093/nar/gkac956
38. Merecz-Sadowska, A.; Isca, V. M. S.; Sitarek, P.; Kowalczyk, T.; Małecka, M.; Zajdel, K.; Zielińska-Bliźniewska, H.; Jęcek, M.; Rijo, P.; Zajdel, R. *Int. J. Mol. Sci.* **2024**, *25*, 4529. DOI: https://doi.org/10.3390/ijms25084529
39. Alecu, I. M.; Zheng, J.; Zhao, Y.; Truhlar, D. G. *J. Chem. Theory Comput.* **2010**, *6*, 2872–2887. DOI: https://doi.org/10.1021/ct100326h
40. Neese, F. *Wiley Interdiscip. Rev.: Comput. Mol. Sci.* **2012**, *2*, 73–78. DOI: https://doi.org/10.1002/wcms.81
41. Dassault Systèmes BIOVIA. Discovery Studio Modeling Environment. Release 2017, San Diego: Dassault Systèmes, **2017**.
42. Dallakyan, S.; Olson, A. J. *Methods Mol. Biol.* **2015**, *1263*, 243–250. DOI: https://doi.org/10.1007/978-1-4939-2269-7_19
43. Abraham, M. J.; Murtola, T.; Schulz, R.; Páll, S.; Smith, J. C.; Hess, B.; Lindahl, E. *SoftwareX* **2015**, *1–2*, 19–25.
44. Huang, J.; MacKerell, A. D., Jr. *J. Comput. Chem.* **2013**, *34*, 2135–2145. DOI: https://doi.org/10.1002/jcc.23354
45. Cuendet, M. A.; Van Gunsteren, W. F. *J. Chem. Phys.* **2007**, *127*, 184102. DOI: https://doi.org/10.1063/1.2779878
46. Uddin, K. M.; Sakib, M.; Siraji, S.; Uddin, R.; Rahman, S.; Alodhayb, A.; Alibrahim, K. A.; Kumer, A.; Matin, M. M.; Bhuiyan, M. M. H. *ACS Omega.* **2023**, *8*, 20247–20256. DOI: https://doi.org/10.1021/acsomega.3c01123
47. Trabelsi, S.; Issaoui, N.; Brandán, S. A.; Bardak, F.; Roisnel, T.; Atac, A.; Marouani, H. *J. Mol. Struct.* **2019**, *1185*, 223–238. DOI: https://doi.org/10.1016/j.molstruc.2019.02.106
48. Petrou, A.; Fesatidou, M.; Geronikaki, A. *Molecules.* **2021**, *26*, 3166. DOI: https://doi.org/10.3390/molecules26113166
49. Shah, P.; Westwell, A. D. *J. Enzyme Inhib. Med. Chem.* **2007**, *22*, 527–540. DOI: https://doi.org/10.1080/14756360701425014
50. Mermer, A.; Bayrak, H.; Alyar, S.; Alagumuthu, M. *J. Mol. Struct.* **2020**, *1208*, 127891. DOI: https://doi.org/10.1016/j.molstruc.2020.127891
51. Zhou, Z.; Parr, R. G. *J. Am. Chem. Soc.* **1990**, *112*, 5720–5724.DOI: https://doi.org/10.1021/ja00171a007
52. Sharom, F. J. *Essays Biochem.* **2011**, *50*, 161–178. DOI: https://doi.org/10.1042/BSE0500161
53. Veber, D. F.; Johnson, S. R.; Cheng, H.-Y.; Smith, B. R.; Ward, K. W.; Kopple, K. D. *J. Med. Chem.* **2002**, *45*, 2615–2623. DOI: https://doi.org/10.1021/jm020017n
54. Shadrack, D. M.; Ndesendo, V. M. K. *Comput. Mol. Biosci.* **2017**, *7*, 1–18. DOI: https://doi.org/10.4236/cmb.2017.71001

J. Mex. Chem. Soc. **2026**, *70(1):e2378*
Regular Issue

ISSN-e 2594-0317

55. Kartsev, V.; Geronikaki, A.; Zubenko, A.; Petrou, A.; Ivanov, M.; Glamočlija, J.; Sokovic, M.; Divaeva, L.; Morkovnik, A.; Klimenko, A. *Antibiotics.* **2022**, *11*, 1337. DOI: https://doi.org/10.3390/antibiotics11101337
56. Babajan, B.; Anuradha, C. M.; Chaitanya, M.; Gowsia, D.; Kumar, C. S. *Int. J. Integr. Biol.* **2009**, *6*, 172–176.
57. Benson, T. E.; Walsh, C. T.; Massey, V. *Biochemistry.* **1997**, *36*, 796–805. DOI: https://doi.org/10.1021/bi962220o
58. Frlan, R.; Hrast, M.; Gobec, S. *ACS Omega.* **2023**, *8*, 36562–36570. DOI: https://doi.org/10.1021/acsomega.3c04813
59. Jain, P.; Guin, M.; De, A.; Singh, M. *J. Phys. Org. Chem.* **2023**, *36*, e4384. DOI: https://doi.org/10.1002/poc.4384
60. De, A.; Ray, H. P.; Jain, P.; Kaur, H.; Singh, N. *J. Mol. Struct.* **2020**, *1199*, 126901. DOI: https://doi.org/10.1016/J.MOLSTRUC.2019.126901
61. Mughal, E. U.; Sadiq, A.; Ashraf, J.; Zafar, M. N.; Sumrra, S. H.; Tariq, R.; Mumtaz, A.; Javid, A.; Khan, B. A.; Ali, A.; Javed, C. O. *Bioorg. Chem.* **2019**, *91*, 103124. DOI: https://doi.org/10.1016/J.BIOORG.2019.103124
62. Kolandaivel, P.; Selvarengan, P.; Gunavathy, K. V. *Biochim. Biophys. Acta, Proteins Proteomics* **2006**, *1764*, 138–145. DOI: https://doi.org/10.1016/j.bbapap.2005.10.016